

## Numerical Modelling of the ‘Bombora’ Wave Energy Conversion Device

A. J. C. King

Fluid Dynamics Research Group,  
 Department of Mechanical Engineering,  
 Curtin University, Western Australia 6102, Australia

### Abstract

This paper presents a numerical model for a novel membrane-based wave energy harvesting device developed by Bombora Wave Power Pty. Ltd. The membrane model was implemented initially implemented in python, followed by a complete implementation as an add-in library to OpenFOAM. The results for 3 configurations of membrane are presented – with  $\Delta p$  of 100, 500 and 1000 Pa, and differing pressure correction terms  $C_p$ . In the presented cases capture efficiencies between 8 and 14% were predicted without any tuning of the PTO parameters, and represent a conservative estimation of the device’s potential.

### Introduction

The Bombora wave energy conversion device represents a new concept for wave energy harvesting[1]. The device consists a number of ‘membrane cells’ connected together and driven by the force of the incoming waves, as shown in Figure 1.

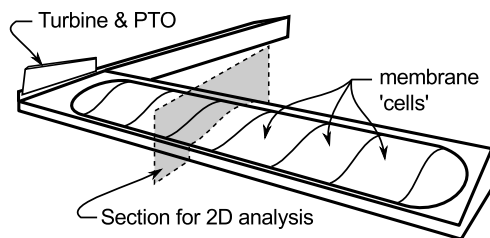


Figure 1. Bombora wave energy conversion device

Each cell operates with a different phase with due to the on-coming wave and in combination the membrane cells are able to drive a near continuous flow of air through the system. Directional check valves at each cell allow flow in one direction through the power take off system as a closed loop. This flow feeds a central air turbine to generate electrical energy.

The device is at its early development stages and characterisation of its performance is required. Typically, wave energy devices have been analysed using a number of techniques, ranging from purely analytical methods[2, 3], numerical methods using linear models[4, 5, 6, 7], full CFD models with and without PTO systems[8, 9], and of course, experimental models. In this work a dynamic model of the membrane cells was developed and integrated into a Computational Fluid Dynamics (CFD) model of the device. Outputs of the model allowed the power output of the system to be quantified given a particular wave condition and parameter setting for the Power Take Off (PTO) unit.

The analysis consists of three parts, the ocean, the membrane, and the power-take-off (PTO) system. The ocean and wave dynamics were modelled using a volume-of-fluid (VOF) approach, while the membrane motion was captured by directly deforming the mesh in accordance with the membrane displacement. The PTO system was modelled as two infinite reservoirs,

with fixed high and low pressures.

The finite volume CFD code OpenFOAM was used as the basis for the modelling. In addition to having well developed mesh motion capabilities [10, 11], the `waves2Foam` extension provides robust wave models within a Volume of Fluid approach[12].

The studies presented in this paper are limited to a 2D-model of the system, which greatly simplified the motions of the membrane. The membrane was discretised into a number of mass-points and their motion was explicitly solved under the action of the applied forces: the local membrane tension, the ‘membrane cell’ pressure, and the hydrodynamic force from the wave. This method was chosen due to its ease of implementation and its robustness. It also allowed the shape and dynamics to be solved in a reasonable amount of time. This was an important consideration as performance modelling of wave energy devices using CFD is computationally costly, and long (physical) times are required to allow device characteristics to be determined. Within this framework the motion of the membrane was easily captured, and the membrane displacement is determined as part of the solution.

### Modelling

#### Fluid Dynamics

The wave motions were modelled using a Volume of Fluid (VOF) approach, where single momentum and continuity equations are solved using phase averaged fluid properties based on a liquid volume fraction ( $\alpha_l$ ) as follows:

$$\frac{\partial \rho \mathbf{U}}{\partial t} + \nabla \cdot (\rho \mathbf{U} \mathbf{U}) = -\nabla P + \mu \nabla^2 \mathbf{U} + \mathbf{F} \quad (1)$$

$$\nabla \cdot \mathbf{U} = 0 \quad (2)$$

An additional transport equation for volume fraction is used to track the free-surface:

$$\frac{\partial \alpha}{\partial t} + \nabla \cdot (\mathbf{U} \alpha_l) + \nabla \cdot [\mathbf{U}_r \alpha_l (1 - \alpha_l)] = 0 \quad (3)$$

Dynamic motion of the mesh was accounted for by solving the momentum, continuity and  $\alpha_l$  equations relative to the mesh by calculating and subtracting a ‘mesh-flux’ (motion of the mesh through the fluid). The above equations are implemented in the standard OpenFOAM solver `interDyMFoam`, which requires the motion of the boundaries to be provided using a suitable boundary condition, described below.

The wave motions were accounted for using the `waves2Foam` [12] extension, which provides a number of tools for defining wave generating and absorbing regions, and boundary conditions for a number of wave theories as well as pre- and post-processing utilities.

#### Membrane

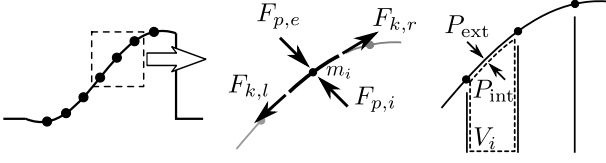


Figure 2. Nodal forces and volume calculation

The characteristics of the (ideal) membrane were such that its behaviour is extremely non-linear – it exhibits very little stretch when under tensile forces, while exhibiting minimal resistance to compressive forces. The loading of the membrane is also strongly dependent on its position due to the hydrostatic pressure acting on the top surface, the internal pressure on the membrane – dependent on whether the cell is inflating or deflating – as well as the wave induced dynamic forces.

The combination of the membrane properties and loading make the problem of determining its shape and motion difficult. To allow the behaviour of the device, the membrane was treated as a series of discrete mass points on which the internal membrane forces and external loads were applied. Figure 2 shows the allocation of forces to an individual mass point.

Face based forces (nominally the pressure forces, but can also include self-weight) were calculated for each segment of the membrane, and allocated evenly to the neighbour nodes as

$$F_{p,e} = \frac{A_l P_{\text{ext},l} + A_r P_{\text{ext},r}}{2} \quad (4)$$

$$F_{p,i} = \left( \frac{A_l + A_r}{2} \right) P_{\text{int}} \quad (5)$$

The only significant node based forces were the membrane tension forces and a membrane damping force. The tension force was calculated as follows:

$$F_{k,r} = EA \left( \frac{|\mathbf{x}_{i+1} - \mathbf{x}_i| - l_0}{l_0} \right) \quad (6)$$

$$F_{k,l} = EA \left( \frac{|\mathbf{x}_i - \mathbf{x}_{i-1}| - l_0}{l_0} \right) \quad (7)$$

where  $l_0$  is the initial unstretched length of each membrane segment. The term  $(|\mathbf{x}_i - \mathbf{x}_{i-1}| - l_0)/l_0$  represents the strain in the membrane material. To account for the reduced capacity for resisting compressive forces the Young's modulus of the material was set to a significantly lower value when the strains were negative. A non-zero value was used partly as the material is able to resist some amount of compression, but also to aid numerical stability. In operation the membrane is typically under tensile forces, so the somewhat arbitrary selection of  $E_{\text{compression}}$  has no impact on the results.

The damping force was included to aid numerical stability, and was calculated as

$$F_{d,i} = -Q_d |\dot{\mathbf{x}}_i| \dot{\mathbf{x}}_i \quad (8)$$

where  $Q_d$  was a damping constant. The value of damping constant was set to a very low value, and the resulting forces were much smaller than the pressure and membrane tension forces. Lack of data for the proposed membrane material did not allow this constant to be set with more certainty.

Explicit integration was used to calculate the motion through time, using a smaller timestep than for the fluid equations. The equations defining the motion of the membrane were implemented as boundary condition to provide the location of the

mesh points making up the membrane. The positions of the internal mesh points were determined by diffusion of the boundary displacements into the internal region of the domain. The boundary condition was created as a separate library dynamically linked at runtime into the solver. Initially, the membrane should be in an unloaded state – correctly this requires that the membrane shape be correct at  $t = 0$  with a calculated initial loading. The calculation of the initial shape is not straightforward, requiring numerical solution of a nonlinear differential equation, based on the hydrostatic loading and membrane tension. After the shape has been calculated, it is required to include this in a suitable form for meshing. As the ‘run up’ length for the wave flume is quite long, it was simpler to solve numerically for the membrane shape as part of the coupled simulation. As such, the initial shape of the membrane was assumed to be a straight line between the end connection points. In this configuration, the lengths of each membrane segment were calculated. These calculated lengths were then scaled to obtain  $l_0$  for each segment, such that the total length of the membrane was correct. Typically, this factor was 1.071 but it was also subject to parametric study.

A python implementation was initially developed to prototype the model prior to a complete implementation within OpenFOAM.

### Backend System

In the 2-dimensional CFD simulations it was only possible to include a single cell of the device, which precluded using a complete power take-off system model. Hence, the cell was assumed to operate between two constant pressure reservoirs determined by a mean pressure,  $P_{\text{mean}}$ , and a operating pressure difference,  $\Delta P$ . This represents an ideal device with an infinite number of cells with uniform distribution of phasing relative to the incoming waves. While this representation is a convenient simplification, it neglects an important factor that allows the device to operate – namely that it is a closed system containing a fixed mass of air. The fixed air mass is important as over long term operation of the device the average position of the membranes across the whole device must remain constant. To capture this in the 2-dimensional models an additional term in was included in the internal pressure equations, to account for drift from the mean membrane position. The complete representation of the pressure in the backend system was

$$P_{\text{internal}} = -C_p V + \begin{cases} P_{\text{mean}} + \Delta P/2 & \dot{V} < 0 \\ P_{\text{mean}} - \Delta P/2 & \dot{V} > 0 \end{cases} \quad (9)$$

where  $V$ , and  $\dot{V} = dV/dt$  are the cell volume, and rate of change of the cell volume. The constant  $C_p$  determined the strength of the restoring pressure provided by the absent backend system.

### Power Output

As only a simplified backend model was used the power was calculated directly from the membrane. At each timestep, the work done on the membrane was determined from

$$W_{\text{timestep}} = \sum_{i=0}^{i=n} (P_{\text{ext}} - P_{\text{int}})_i \Delta V_i \quad (10)$$

Where  $V_i$  is the change in the internal volume between two adjacent mass points. The average power capture potential for a given time interval was then

$$\dot{W}_{\text{avg}} = \frac{\sum_{t_s}^{t_e} W_{\text{timestep}}}{t_e - t_s} \quad (11)$$

Case	$\Delta P$ [Pa]	$P_{\text{mean}}$ [Pa]	$C_P$ [Pa/m <sup>3</sup> ]
A	1000	38396	-1000
B	100	38396	-100
C	500	37396	-2000

Table 1. Presented cases

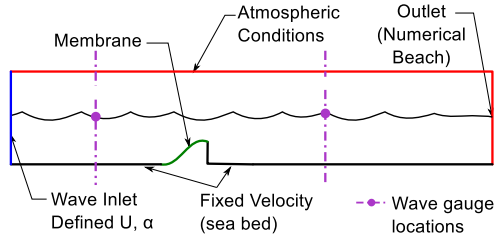


Figure 3. Arrangement of the 2D simulations

### Case Setup

Figure 3 shows a representation of the domain, as well as applied boundary conditions. Three cases are presented with different PTO settings as listed in Table 1. Simulations for these cases were conducted using the same membrane settings for stiffness,  $k_t = 1 \times 10^{11}$ , and length ratio,  $l_{\text{act}}/l_{\text{initial}} = 1.071$ . The wave conditions for all were also kept constant with  $H_w = 1.0$  m,  $T_w = 6.57$  s, and a water depth of 5 m. This combination falls within the second order Stokes region for the applicable wave theory.

### Results

#### Membrane Shape & Volume

Figure 4 shows the initial shape of the membrane, as well as shape at the minimum and maximum volume over one cycle for Case A. Figure 5(a) shows the deviation in volume (initially at zero) during the simulation. From this figure, it is clear that the mean volume of air within the modelled device does not stay at zero, and is sensitive to the PTO settings. Case A and B are gradually inflating, while Case C is deflating. This characteristic of the model is discussed later.

#### Power Output

Figure 5(b) shows the time-averaged power output from the model for each of the three cases. In each case there are some initial transients present due to the setting the initial profile to be straight. After approximately 15 s, the effect of the ini-

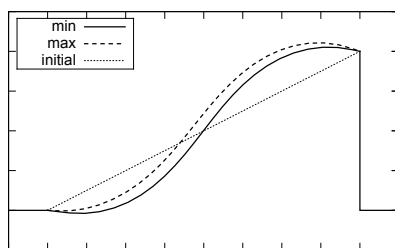


Figure 4. Developed membrane shape at minimum and maximum volume, compared with initial shape

tial ‘stretching’ of the membrane is not present, and the average continuous power output can be determined. The predicted continuous operating power outputs of the device were 793 W, 677 W and 1233 W respectively. The corresponding power in the incident wave per meter width can be calculated from

$$\dot{W}_w = \frac{\rho g H_w^2 c}{8} \quad (12)$$

which for the current wave conditions is 8.85 kW. This corresponds to capture efficiencies between approximately 8% to 14.1%, though it is important to note that these cases are far from the optimal settings and much better performance is expected to be observed with an optimised set of membrane and PTO parameters.

### Discussion

#### Cell volume

The long-term change in cell volume is an obvious characteristic of the results, and warrants some explanation. If  $P_{\text{mean}}$  is too high the cell gradually inflates, while when too low, the cell deflates. For a single cell model, operating around a mean volume deviation of zero is not stable – if  $P_{\text{mean}}$  is slightly above the required setting the membrane inflates slightly and the average hydrostatic static pressure on the external surface of the membrane decreases. This in turn allows the membrane to further inflate. A similar effect occurs when  $P_{\text{mean}}$  is slightly lower than it should be. In both cases the membrane does reach a stable state being either fully deflated or fully inflated. This behaviour is a consequence of the 2D model, in a complete model of the device there is a fixed mass of fluid within the working sections (membrane cells, connecting ductwork and accumulators). This means that across the device there is no accumulation or reduction in fluid, and if the membrane cells are identical their average volume will remain constant. This effect is partially countered by the addition of the  $C_P$  term which is able to be adjusted to maintain a constant average volume.

#### Power output

The presented results show that the device is capable of capturing a reasonable amount of wave energy (15%) even for the untuned device. As with most generation devices it is expected that there will be a single optimum operating point for a given wave condition, representing a trade-off between the operating volume change and pressure difference. The limits of this operation are naturally no pressure difference and maximum motion, and maximum pressure difference and no motion. Where the current results sit in relation to the optimum is unclear, but will be determined through more detailed parametric study on the operating pressures and membrane characteristics (mass and length). These results will also be used to give insight to parameter ranges to be used in upcoming tank-testing.

#### Validation

The results presented here are yet to be comprehensively validated, with quantitative validation limited to the performance of the wave flume domain and CFD models. At this point, only qualitative validation of the membrane and PTO has been undertaken. Primarily this due to a lack of detailed experimental data on the operation of the Bombora device. Given this state - this work was undertaken as preliminary work to evaluate whether the operating principles of the device are sound, and the commercial viability of tank testing. Tank testing of the device is to commence in the near future, and the data gained allow the results from this model to be more comprehensively validated.

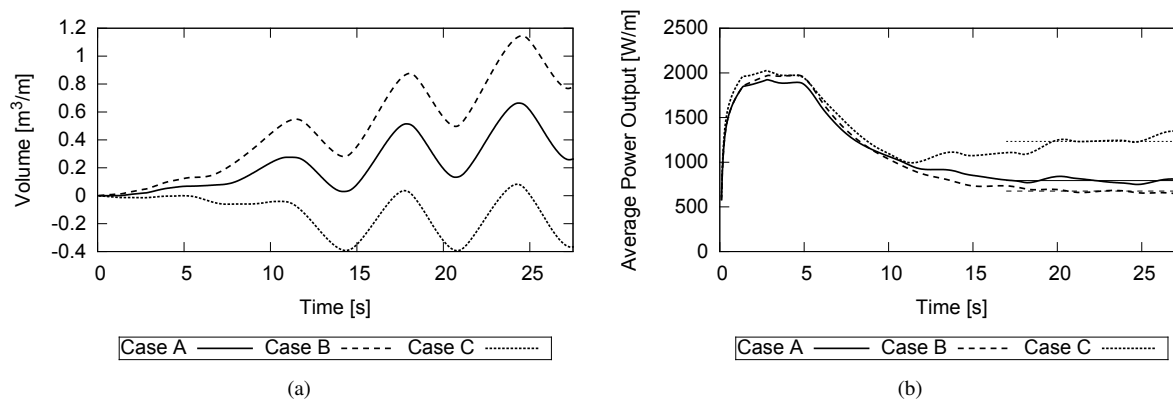


Figure 5. Results for  $T = 6.57s$ ,  $H = 1.0$

### Other modelling

The numerical model presented in this paper was initially developed on the assumption that methods using linear wave theory may not be able to accurately model the operation of the device. This was due to uncertainty of the membrane shape when operating, the potentially large displacements that may be observed, and the relative size of the device when compared with the water depth. As this model has provided some insight into these questions linear modelling of the device is being undertaken (by others) to test this assumption and to allow some optimisation of the device parameters to be performed. The linear wave theory modelling should allow a larger parameter space to be searched as results are able to be generated significantly faster.

### Conclusions & Further Work

The presented model is able to predict the potential power capture capability of a wave energy conversion device similar to the Bombora design. The three operating cases presented in this paper predicted operating capture efficiencies up to 14% with no tuning, and for a single wave condition with an incident height of 1.0 m, and a period of 6.57 s. The model was also able to determine the shape of the membrane during operation using a simplified method of initialisation. A key limitation of the model was that a simplified model of the backend system was necessary as a consequence of treating the problem 2-dimensionally. A pressure correction term,  $C_p \Delta V$ , was added to the mean operating pressure to account for drift in the operating volume in the simplified model, but further optimisation of this term is required.

To better model the device, a similar membrane model to that described in this paper is being developed using a full 3-dimensional model of the membrane with separate cells, in addition to a more complete backend that negates the need for the  $C_p$  term.

### References

- [1] URL <http://bomborawavepower.com.au/>.
- [2] M. Eriksson, J. Isberg, and M. Leijon. Hydrodynamic modelling of a direct drive wave energy converter. *International Journal of Engineering Science*, 43(17–18): 1377–1387, 2005. ISSN 0020-7225.
- [3] Johannes Falnes. A review of wave-energy extraction. *Marine Structures*, 20:185–201, 2007.
- [4] J M B P Cruz and S H Salter. Numerical and experimental modelling of a modified version of the edinburgh duck wave energy device. *Proc. IMechE: Part M: J. Engineering for the Maritime Environment*, Vol. 220:129–147, 2006.
- [5] M.F.P. Lopes, J. Hals, R.P.F. Gomes, T. Moan, L.M.C. Gato, and A.F.de O. Falco. Experimental and numerical investigation of non-predictive phase-control strategies for a point-absorbing wave energy converter. *Ocean Engineering*, 36(5):386 – 402, 2009. ISSN 0029-8018. doi: <http://dx.doi.org/10.1016/j.oceaneng.2009.01.015>.
- [6] Gregory S. Payne, Jamie R.M. Taylor, Tom Bruce, and Penny Parkin. Assessment of boundary-element method for modelling a free-floating sloped wave energy device. part 1: Numerical modelling. *Ocean Engineering*, 35:333 – 341, 2008. ISSN 0029-8018.
- [7] Pedro C. Vicente, Antnio F. de O. Falco a, and Lus M.C. Gatoand Paulo A.P. Justino. Dynamics of arrays of floating point-absorber wave energy converters with inter-body and bottom slack-mooring connections. *Applied Ocean Research*, 31:267–281, 2009.
- [8] Christopher Caskey and Tiger Jeans. Analysis of a cycloidal wave energy converter using unsteady reynolds averaged navier-stokes simulation. In *Proceedings of the 10th European Wave and Tidal Energy Conference*, 2013.
- [9] Johannes Palm, Claes Eskilsson, Guilherme Moura Paredes, and Lars Bergdahl. Cfd simulation of a moored floating wave energy converter. In *Proceedings of the 10th European Wave and Tidal Energy Conference*, 2013.
- [10] OpenFOAM Foundation. *OpenFOAM - User Guide*. OpenFOAM Foundation, December 2011. Version 2.1, <http://www.openfoam.org/>.
- [11] H. Jasak and Z. Tukovic. Automatic mesh motion for the unstructured finite volume method. *Transactions of FAMENA*, 30(2), 2007.
- [12] N G Jacobsen, D R Fuhrman, and J Fredsøe. A Wave Generation Toolbox for the Open-Source CFD Library: OpenFoam®. *Int. J. Numerl. Meth. Fluids*, 70(9):1073–1088, 2012. doi: 10.1002/fld.2726.